Multi-scale particle morphology evolution in rotating drum tests: role of particle shape and pore fluid

Ting Yao[1], Hongwei Yang[2], Sérgio D.N. Lourenço[3*], Beatrice A. Baudet[4], Fiona C.Y Kwok[3]

1. Institute of Rock and Soil Mechanics, Chinese Academy of Sciences, China
2. School of Civil Engineering, Sun Yat-sen University, Guangzhou, China
3. Department of Civil Engineering, The University of Hong Kong, Hong Kong
4. Department of Civil, Environmental and Geomatic Engineering, University College London, U.K.

*Corresponding author (lourenco@hku.hk)

Abstract

During the downslope long-distance movement of debris avalanches, particles interact with each other in various modes, by rolling, sliding and colliding with each other. During transport, grains may undergo breakage, changing in size and shape. However, research on debris avalanches at the grain scale remains limited, in particular, the evolution of grain morphology at different scales, from the overall form down to surface roughness, with runout distance. This paper investigates the evolution of particle morphology of granite gravel particles during long distance travel using a rotating drum, Micro-Deval apparatus, together with three-dimensional (3D) image analysis with a 3D laser scanner. The effects of particle shape and pore fluid (dry, saturated with water or slurry) on the evolution of particle morphology during transport were investigated. It was found that while the gravel was strong enough to resist the fragmentation that could be induced by the inter-particle actions during testing, the corners and edges became rounded, and the general form and surface roughness remained unaffected by the particle interactions. The more angular the grains, the easier the corners to be abraded during interaction. The change of local roundness of the grains was amplified in water-saturated conditions and suppressed in a slurry-saturated medium. The viscosity of the pore fluid, rather than initial particle shape, was critical in controlling the particle morphology evolution.

Keywords: Debris avalanches; 3D particle morphology; pore fluid

1. Introduction

Debris avalanches are very rapid to extreme rapid shallow flows of partially or fully saturated debris on a steep slope, without confinement in an established channel, according to the classification of landslide proposed by Cruden & Varnes (1996) and updated by Hungr et al. (2014). They involve the movement of a mass of boulders, gravel, sands, and fines in water down a slope (Cruden, 1991). Soil grains interact by colliding, sliding, or rolling during their long-distance runout and are subject to damage as a result. Damage can evolve at different scales changing particle morphology during transport through breakage and abrasion. Particle breakage may change the size and form. Therefore, small sized particles can fill the gap between large particles and thereby reduce the saturated permeability within the shear zone, generating excess pore water pressure and reducing the effective stress, which weakens the frictional resistance at the particle contacts (Sassa, 1998; Agung *et al.*, 2004; Davies & McSaveney, 2009; Chen & He, 2020). Damage can also develop in the form of abrasion at the asperities which may cause angular particles to become rounded, and occur at the micro-scale, smoothening surfaces and reducing the friction angle (Zuo *et al.*, 2019). As a result, the mobility and runout of rainfall-induced debris avalanches are enhanced (Iverson, 2003).

Particle damage may evolve in different modes during transport depending on the interactions between granular solids and the characteristics of pore fluid (air, water, slurry). An experimental investigation of the particle breakage of sand grains in granular flow in dry condition (*i.e.,* pore fluid is air) found that the interactions between particles are mainly friction and collision. As a result, the particle damage mechanisms are mainly dominated

by abrasion and splitting, respectively (Yu *et al*., 2020). The cushion effect of clay in fines-rich landslides is traditionally expected to inhibit significant particle breakage induced by collision. However, particle breakage has been reported in fines-rich landslides (Gerolymos & Gazetas, 2007). Caballero *et al.* (2012) studied the fracturing and comminution of gravel and sands (andesite in composition) in debris flows using a Los Angeles abrasion apparatus, with tests conducted with pore fluids made up of silt and clay rich slurries, and particle morphology was quantified by two-dimensional image analysis. The test results showed that the silt content mainly affected the change of roundness, while the presence of clay reduced surface texture. This, however, was not found in a recent study of a submarine landslide which is assumed to be fully saturated, where Li *et al.* (2019) found that the particle morphology, mostly dominated by silt-sized fraction, was not influenced by the movement of the marine deposits. Therefore, questions remain on the evolution of particle morphology (size and shape) and its interplay with the pore fluid, *i.e.*, composition of fines and water content. The particle morphology needs to be accounted for across several scales, as demonstrated by Caballero *et al.* (2012), from the form down to surface texture.

In this paper, we present a systematic study on the morphological evolution of gravel particles during long-distance travel where the three scales of morphology, *i.e.*, surface roughness (smooth or rough), local roundness (the sharpness of the corners, angular or rounded) and general form (global shape, elongated or spherical) (Figure 1) were mapped at different runout distances simulated by drum tests. The impact of particle shape and pore fluid was investigated through tests performed on rounded and angular gravel particles in dry condition, saturated with water and, saturated with a slurry made of clay or silt. The

morphology was quantitatively characterized for increasing number of revolutions for each particle, based on three-dimensional (3D) image analysis obtained by laser scanning following a method recently proposed by Yang *et al.* (2019).

2. Methodology

2.1 Rationale

With the aim of investigating the morphology evolution of gravel particles in debris avalanche movement, a series of rotating drum tests, with 3D image analysis by a 3D laser scanner, were carried out. Rotating drum tests have long been adopted to simulate a continuous stationary granular flow analogue to debris avalanches and flows (*e.g.*, Longo & Lamberti, 2002; Kaitna & Rickenmann, 2007; Schneider *et al*., 2011; Caballero *et al.*, 2014). Here, the debris avalanches were simulated in a Micro-Deval apparatus, a widely used test to determine the abrasion resistance of aggregates (*e.g.*, Masad *et al*., 2011; Allam & Ebrahimpour, 2014; Czinder *et al*., 2021). The working principle consists of placing a dry granular sample mixed with water and a charge of steel balls into the stainless-steel drum. The rotation of the drum allows a continuous flow where grains undergo physical degradation by colliding or sliding against each other and by the interactions with steel balls and steel drum. Despite the possibility of segregation due to the density difference between the gravel and the steel balls, the purpose of using steel balls is to accelerate degradation. Lin & Lourenço (2020) demonstrated that the mass loss of sands (98% quartz) undergoing rotating drum tests without steel balls is negligible. The drum was rotated at a given speed of 100 rpm (revolution per minute), and travel distances were estimated to be approximately up to 7 km and 22 km, which were thought to be long enough to reach a

stable morphology (*e.g.*, distances of 11-20 km were suggested by Caballero *et al.* (2012)).

Debris avalanches in Hong Kong are known to have a grain size distribution ranging from clay to gravel, with coarser fractions dominating the mixtures. For instance, the Tsing Shan event (Ng *et al*., 2021), was dominated by gravel (75%) with the remaining fractions comprising sand, silt, and clay. For easy identification of the morphology evolution of every single particle, gravel with particle size of 20-30 mm sorted by sieving analysis was used. The gravel is unweathered (fresh) crushed granite collected from a quarry in Hong Kong, made up of biotite, plagioclase feldspar and quartz, and its chemical composition comprises 70-77% silica (SiO_2) by weight (Sewell, 1999).

To assess the effect of particle shape, tests were conducted in a dry condition on rounded (RUN 1) and angular particles (RUN2) (Figure 2). According to the classification of landslide proposed by Cruden & Varnes (1996) and updated by Hungr *et al*. (2014), RUN 1 and RUN 2 could replicate the particle interactions during dry debris avalanches. One gravel-water mixture (RUN 3), one clay-slurry mixture (RUN 4), and one silt-slurry mixture (RUN 5) were also tested to investigate the influence of the pore fluid viscosity (water, silt, or clay rich slurries) on the particle interactions in debris avalanches. The testing conditions are summarized in Table 1. The solid concentrations by volume for RUN 3 to RUN 5 cover the range from dilute to dense flows (Iverson & George, 2014). Although RUN 3 is not classified as a debris avalanche according to the terminology used by Iverson & George (2014), it allows a comparison with other RUNs (RUN 4 and RUN 5) to investigate the influence of pore fluid (water, clay, or silt rich slurries) on the particle

interactions.

Since it has been suggested that more than 20 particles are required to study soil grain morphological features (Altuhafi & Coop, 2011), 32 grains were used for each test. Each grain was numbered so that its morphology could be tracked before and during testing. RUN 2 to RUN 5 were made of the same number of angular gravel particles (386.0 g, 361.1 g, 395.3 g, and 377.1 g for RUN 2 to RUN 5) but different percentages of water, clay and silt (Table 1). To investigate the influence of the plasticity of fine sediment on the particle interaction in debris avalanches, slurries composed of water and commercially available kaolin clay (d_{50}=5 μm) and non-plastic crushed silica (d_{50}=20 μm) (Zheng *et al.*, 2019) were used for RUN 4 and RUN 5, respectively. The water content of the slurry of RUN 4 is close to the liquid limit of kaolin as adopted by Jing *et al.* (2018) and the same water content is used for the silt-water mixture of RUN 5.

2.2 Instrumentation and testing programme

2.2.1 Micro-Deval testing

Testing was performed in a rotating drum (Micro-Deval apparatus) as shown in Figure 3. The drum has an inner diameter of 200 mm and rotates along its horizontal axis at 100 rpm (revolution per minute). Although the total mass of the five tests varied from 1351 g to 2303 g (Table 1), the modified Froude number proposed by Juarez *et al* (2011) which takes the volume fill fraction into consideration of the 5 RUNs is within the same magnitude. Based on the *Bed Behavior Diagram* proposed by Mellmann (2001), the type of particle movement of all RUNs is similar. In addition, Ngan-Tillard *et al* (2009) found that the

degradation of sand particles during Micro-Deval test is mainly influenced by the mass ratio between sand and steel balls. Therefore, the major factor affecting the damage of gravel during rotation should be the mass ratio between the gravel and the steel balls. The ratio between the inner diameter of the drum and d_{50} of the gravel (approximately 8) is similar to the rotating drum tests carried out by Caballero *et al.* (2014) and Arabnia (2015).

For each test, (1) gravel was oven-dried and numbered with an oil marker; (2) each grain was then weighed and scanned by the 3D laser scanner to obtain the morphological parameters prior to the test; (3) the mixtures, corresponding to the set conditions above (RUN 1 to RUN 5) were then placed into the drum and mixed with steel balls with a mass ratio of 2.5 (steel balls to gravel), and the mass of steel balls for each RUN is listed in Table 1. For each RUN, the mixtures were subjected to two consecutive intervals of 20000 and 40000 revolutions, making a total 60000 revolutions (Figure 4). The travel distance of granular flows is commonly calculated by the product of the circumference of the drum by the number of revolutions. However, it has been demonstrated that the actual travel distance is overestimated by this method (Lewin & Brewer, 2002). Following Adams (1978), the travel distance was calculated as 60 percent of the drum circumference per revolution, resulting in estimated travel distances of approximately 7.2 km and 22.6 km for 20,000 and 60,000 revolutions, respectively. After each rotation period, the mixtures were wet sieved to remove the fines (smaller than 0.063mm) and to determine the mass loss of the gravel. The coarse fractions collected by sieving after each rotation period were oven-dried and scanned for analysis. After the first rotation period, the same gravel sample was then placed into the drum with the steel balls for the second rotation period, assuming that the removal

of fines between the two rotation stages did not affect the damage mechanisms significantly. A total number of 480 grains were therefore scanned (five tests, 32 grains for each test, before and after each rotation period).

2.2.2 3D laser scanning

Three-dimensional (3D) laser scanning is an effective method to quantify the morphology of coarse granular materials such as aggregates (Lanaro & Tolppanen, 2002) and gravel (Yang *et al.*, 2019; Yang *et al*., 2020) or ballast (Anochie-Boateng *et al.*, 2013). A 3D laser scanner (LPX-60, Roland DG Corporation, Hamamatsu, Japan) capable of measuring particle size up to 203 mm diameter and 304.8 mm height was used. The highest resolution was 0.2 mm/scanning pitch vertically and 0.2 mm/degree circumferentially. The plane scanning mode, which scans the particles from four directions, was selected. Before scanning, each grain was fixed on a holder with double sticky tape to avoid movement. In order to minimize the unscanned areas on the grains, the contact area between the grain and the holder was kept as small as possible. The four scanned planes were merged by the in-built software (Dr. PICZA3) to generate a 3D model of each grain. Care was taken to place the grains in the same orientation for scanning before and after each rotation period.

2.2.3 3D particle morphology analysis

The gravel morphology was determined by 3D image analysis at three scales: form (overall shape), roundness and surface roughness as proposed by Barret (1980) and Blott & Pye (2008). Form represents the proportions of the particle at the macro-scale. Roundness reflects the local features of the corners at meso-scale, and roughness accounts for the

surface texture of the particle at micro-scale (Mitchell & Soga, 2005; Cho *et al.*, 2006).

Parameters which represent the form are associated with the three principal dimensions of a box containing the particle: the major axis (L), intermediate axis (I) and minor axis (S). The orientations of these three axes for each particle was determined by the principal component analysis (PCA) on the vertexes of the 3D particle model, which has been applied to the study of tomographic characteristics of grains (Fonseca *et al.*, 2012). Here, we used average particle size defined as the mean of the three principal dimensions. Two aspect ratios, the elongation index (EI) and the flatness index (FI), which are defined as EI=I/L and FI=S/L, were used to quantify the overall form of gravel grains.

The 3D local roundness R, which defines the 3D corners as the parts of the particle surface having larger local curvature values than its maximum inscribed sphere, was used in this study (Zhao & Wang, 2016) and is expressed as:

$$R = \frac{\sum\left(A_n \frac{k_s}{k_M}\right)}{\sum\left(A_n\right)} \tag{1}$$

where A_n is the area of the n^{th} triangular element of the reconstructed surface by triangular meshes; k_s is the curvature of the maximum inscribed sphere of the particle and k_M is the mean curvature of the maximum and minimum principal curvatures of a vertex. As a reference, Zhao & Wang (2016) found that the average value of the roundness for the Leighton Buzzard sand particles with size of 1-2 mm is 0.71.

The surface roughness of gravel can be quantified at the millimeter scale by the 3D laser

scanner with resolution of 0.2 mm/scanning pitch, as described in Yang *et al.* (2019). Surface roughness is usually quantified by the square root of the surface heights to a mean plane S_q (*e.g.*, Otsubo *et al.*, 2015; Yao *et al.*, 2019; 2021) or the fractal dimension (*e.g.*, Yang *et al.*, 2016). Although S_q has been frequently used because of its simplicity, it has been proved to be resolution dependent. Therefore, Yang *et al.* (2019) proposed to characterize the surface roughness of gravel-sized grains by the scale-independent fractal dimension, the Power Spectrum Density (PSD) method, enabling tracking the change of surface roughness after each rotation period. The PSD is defined as (Nayak, 1971):

$$PSD\left(q_x, q_y\right) = \frac{1}{\left(2\pi\right)^2} \int\int_{-\infty}^{\infty} A\left(x, y\right) e^{-i\left(xq_x + yq_y\right)} dxdy \tag{2}$$

where $A(x,y)$ is the auto-correlation function of surface height and q is the wavevector (in mm^{-1}). The surface of the grains is assumed to be isotropic where the PSD (q_x, q_y) could be reduced to PSD(q) by the angular average of the wavevector. PSD follows a power law when $q \geq q_c$, where q_c is the cut-off wavevector that is associated with the maximum inscribed radius of the particle R_{ins} and is expressed as (Yang *et al.*, 2016):

$$PSD\left(q \geq q_c\right) = C_0 \left(q / q_c\right)^{2D_{PSD}-8} \tag{3}$$

where D_{PSD} is the fractal dimension related to the slope of the straight fitting line in the double logarithmic plane of PSD versus q and C_0 is related to the intercept. D_{PSD} was used to characterize the surface roughness of the grains. The higher the D_{PSD} is, the rougher the surfaces are. Yang *et al.* (2019) found that the D_{PSD} of the same gravels with the particle size of 5-10 mm and 10-20 mm was around 2.57.

2.2.4 Characterization of testing materials

From the data generated by the laser scanning tests, the mean values of the mass, particle size, aspect ratios, roundness, and fractal dimensions were obtained. The values for 32 grains selected for each run prior to testing are summarized in Table 2. The particle size of a gravel grain was determined by the mean value of the three-principal dimension (L, I, S) introduced above. A mean diameter d_{50} of approximately 24 mm was determined for each sample. Figure 5 shows the aspect ratios of the gravel of each RUN, and according to the classification proposed by Zingg (1935), most grains could be classified as "spheroid" as both EI and FI are larger than 2/3. The roundness R of the grains varies from 0.60 to 0.62, and mean values of D_{PSD} are within the range of 2.50 to 2.60.

3. Results

3.1 Effect of particle shape

RUN 1 and RUN 2 were carried out to investigate the effect of particle shape on its morphology evolution. Figure 6 presents the decrease in percentage of the mass of gravel in RUN 1 and RUN 2, and the error bars in the figure represent the standard deviations. The mass loss of RUN 2 is more significant than RUN 1 throughout both rotation periods, as the corners of angular particles are more vulnerable to breakage. The mass loss of both RUN 1 and RUN 2 reduces after the first rotation period as particles get rounded and are more resistant to breakage. By the end of the test, the percentages of mass loss are around 5% and 8%, for RUN 1 and RUN 2, respectively. After each rotation period, fine grey powder was observed on the surfaces of the grains, the steel balls and inside the steel drum wall. Particle breakage was not identified but comminution is evidenced by the fine grey

powder.

Figure 7a shows the evolution of the same grain from RUN 1 at different rotation stages. Although the grain is recognizable at the end of the test, with its general form preserved, the initial sharpness of corners has been significantly reduced. Its mass loss was estimated to be less than 0.5 g after 60000 revolutions, which is insignificant to the initial mass of the grain. The quantifying parameters representing the general form, EI and FI, remained unchanged, while the estimated roundness showed an increase from 0.67 to 0.70, as the sharp corners of the grain were progressively rounded. The fractal dimension, D_{PSD}, representing the surface roughness, was not sensitive to the particle interactions.

The particle breakage, which mostly consisted in the abrasion of the corners of the grain, did not have a significant effect on the particle sizes in RUN 1 and RUN 2 (Figure 8a). The evolutions of roundness and fractal dimension, shown in Figure 8b, confirm that roundness increases with the number of revolutions in both RUNs, more prominently for the angular ones as the corners of angular particles are more vulnerable to breakage (RUN 2). These results indicate that the gravel had the ability to resist breakage mainly due to its unweathered nature and its high quartz content with uniaxial compression strength likely to be 150-350 MPa (Lumb, 1983), so that while the roundness changes, the overall form of the grains was not affected by the flow. The fractal dimensions were not affected in either run (Figure 8b). The mean values of the morphological parameters determined before and after each rotation period for all samples are summarized in Table 2.

3.2 Effect of pore fluid

The decrease of the gravel mass for RUN 2 to RUN 5 with increasing number of revolutions is presented in Figure 9a. All samples in RUN 2 and RUN 5 had a similar initial form, roundness and fractal dimension. The reduction in mass is more prominent during the first period of rotation for all runs, as the sharp corners of the gravels have been rounded during the first rotation period. This is comparable to the effect of particle shape in section 3.1. At the end of the test, the decrease in the percentage of the mass of each sample varies from 2% to 12%. The percentage of the mass loss of RUN 3, where the gravel is saturated with water, is the highest (12%). The percentages in the mass loss of RUN 4 and RUN 5, which contained fines in the mixtures, are 2% and 5%, respectively, which are less than that of RUN 2 (8%) where the grains were tested in a dry condition. There is evidence of more intensive particle interaction in RUN 3 as several grains with particle size of 2-3 mm were created, while only grains finer than 0.063 mm were produced for the other RUNs. Accordingly, the grains of RUN 3 had the most significant reduction in average particle size, from 24.00 mm to 21.84 mm by the end of the test, correlating with the mass loss.

The grain experienced maximum change of morphology was also found in RUN 3 (Figure 7b). By the end of rotation, its percentage of the mass loss is as high as 30%. As a result, its diameter decreases from 23.87 mm to 19.73 mm, while the change of general from is insignificant. The roundness increased from 0.62 to 0.71, as the angular corners have been significantly rounded by gravel-gravel and gravel-steel ball interactions. The surface of the grain is visibly smoothened, and the fractal dimension decreases from 2.563 to 2.519. By comparison, the other RUNs showed a negligible decrease in particle size with increasing

number of revolutions. As a result, the samples show insignificant variations in form according to Zingg's diagram as shown in Figure 9b (RUN 2 to RUN 5).

The evolutions of roundness for RUN2 to RUN 5 are shown in Figure 9a. Although the general form of the grains remains the same, the roundness of these grains increases during the test, producing more rounded grains. Increases in the roundness of the gravel are more pronounced at the first stage (up to 20000 revolutions). At the end of the test, *i.e.* 60000 revolutions, the gravel tested in dry (RUN 2) and saturated (RUN 3) conditions underwent the highest increment of the roundness (0.61 to 0.67). During the first rotation period, the roundness of the gravel for RUN 3 increased most rapidly (0.609 to 0.650), while the increase rate decreased at the second stage of tests which is much lower than that of RUN 2. The increase in roundness of samples for RUN 4 and RUN 5, which were slightly rounder than the other samples, was much lower, possibly due to the presence of fines in the mixtures. For example, RUN 4, where the gravel mixed with clay was subjected to the lowest increase in roundness.

The fractal dimensions for the samples (RUN 2 to RUN 4), shown in Figure 9a, presented a decreasing trend with increasing number of revolutions, but these changes are insignificant. Only the fractal dimension of RUN 5 (silt-based slurry) increased firstly and then decreased with increasing number of revolutions, indicating that the gravel surface may have become slightly more irregular by the end of the test.

4. Discussion

Mixtures of particles with different size and density can either segregate or mix during flow. In a mixture of smaller heavy particles with larger lighter particles, both buoyancy and percolation act together, leading to the formation of a core made of the heavier particles surrounded by larger lighter particles. However, this strictly depends on a variety of factors, from ratio of particle sizes and ratio of density sizes to angular velocity, among others. In a similar study conducted by Jain *et al*. (2005), glass beads (3 mm) and steel balls (1 mm) were subjected to 1, 4, 8, 16 rpm in a rotating drum. As the rotation speed increased, the formation of radial streaks at 1 rpm was replaced by a 'classical' segregated core made of steel balls at 16 rpm. Establishing a parallel with our study, the density ratio is the same (2.65 for gravel versus 7.5g/cm^3 for steel balls), the diameter ratio is comparable (10 to 22 mm in our study) but the rotation speed is considerably higher in our study (100 rpm to 16 rpm). At such a high rotation speed, whether it translates into segregation or mixing, remains unknown. In similar rotating drum tests in binary mixtures, Santos *et al*. (2016) found that radial segregation induced by size differences is less significant with increasing rotation speed. The study has the added complexity of using gravel with an irregular shape and different pore fluids. The uniform degradation of the gravel for all runs, suggests, at least, some degree of mixing with the steel balls and gravel interacting with each other. This is further corroborated by the fact that there is no mass loss for gravel-only mixtures in the rotating drum.

In all RUNs, a limited change of general form, which corresponds to the macroscale of the particle size, was observed in spite of differences in the angularity of the grains and the property of the pore fluid (air, water and slurry). The dominant factor in the damage (or

lack of damage) at that scale was the particle strength of the tested gravel which was high enough to resist fragmentation.

Differences in damage could be observed at the meso-scale of particle morphology, with the roundness of the gravel increasing with the number of revolutions, suggesting abrasion to the edges. For all RUNs, the increase of roundness of the gravel was more significant during the first rotation period, which means that the particle morphology modification at the meso-scale weakened with increasing runout. The pore fluid seems to influence that stage of damage, with visible differences in the propensity for abrasion in the different RUNs. In dry conditions (RUN 1 and RUN 2) the rolling and sliding between grains generate fines which could have formed a cushion (Woodside & Woodward, 1998; Lin & Lourenço, 2020), damping the impact of the steel balls between particles as shown in Figure 10a. In RUN 3, on the one hand, the viscosity of water reduces the grain dynamics during rotation (Chou *et al.*, 2014), thus the intensity of particle interactions decreases. On the other hand, when grains were saturated with water, the fines created during rotation were dispersed in water (Figure 10b), enhancing the wearing and abrasion between them. The grains mixed with fines as slurry (RUN 4 and RUN 5) experienced lower increases of roundness compared to the samples tested without fines. This may be attributed to the cushioning effect induced by the high content of silt and clay in the mixtures (Figure 10c), which would have inhibited collision between grains (Caballero *et al.*, 2012), and therefore postponing the rounding of the corners and edges of the gravel grains. The silt grains, made of crushed silica are non-cohesive, thus most of them were suspended in water during rotation (Figure 10d). By contrast, clay platelets may have gradually coated the surfaces of

the gravel during rotation, bonded by van der Waals forces and hydrogen and cation bonds (Ansari *et al.*, 2003). Consequently, the cushion effect of the silt-rich slurry would be less significant than the clay-rich slurry.

The irregularities of the surfaces, which could be captured by the microscale morphological parameter that is the fractal dimension (Yang *et al.*, 2019), present an insignificant decreasing trend with increasing number of revolutions except for the gravel in a silt-based slurry (RUN 5). The material used in this work is a coarse-grained and freshly crushed granitic rock and is therefore relatively resistant to surface scratches and abrasions. The difference in the particle size and nature of silt and clay results in different effects on the modification of the morphology at meso- and micro- scale. Silt, made of crushed silica (with angular shape and high hardness), fills the space between particles, enhancing the abrasion effect as the gravel and steel balls roll, collide and shear against each other, ultimately rounding the edges and corners to increase roundness.

The findings of this work provide an insight into the understanding of the mobility of the long runout debris avalanches. Although particle breakage of granite gravel is limited, the corners of the particles have been rounded under all test conditions. Debris avalanches involve the movement of boulders, gravel, sands, and fines. Perinotto *et al.* (2015) carried out a field study on the change of morphological properties of the debris avalanche deposits of La Réunion Island (0.5-300 mm) with run-out distance, and a morphological syn-transport evolution is clearly identified for the isolated clasts (0.5-50mm) with particles becoming more rounded and circular with increasing run-out distance. Therefore, it can be

concluded that the roundness of the coarse-grained debris avalanche deposits increases with downslope movement. It implies that during the downslope movement, the apparent friction angle of the gravel might be reduced due to the increase of particle roundness (Cho *et al*., 2006; Rousé *et al*., 2008), which in turn enhances the mobility of debris avalanches. The nature of pore fluids affects the impact between particles which further influences the change of roundness of gravel during the debris transport. The more cohesive the fines in the pore fluid are, the less the change of roundness of the gravel. Particle breakage can be caused by other mechanisms in large scale debris avalanches, for example, due to the high shear rate and confining pressure at the base which is not considered in this study and deserves further investigation.

5. Conclusions

The effects of pore fluid and particle shape in granular flows have been investigated through laboratory rotating drum tests on both rounded and angular gravel, carried out in a Micro-Deval apparatus. The soils tested were either dry, saturated with water or saturated with a clay and silt suspension, while travel distances simulated varied between 7 km to over 20 km. Abrasion was found to be the main particle damage mechanism in the dry specimens, especially on the more angular grains. This created fines which coated the particles and provided cushioning so that abrasion ceased. In the fully saturated samples, the fines were removed from the surface of the gravel grains and further abrasion was observed. When the fines in the pore fluid are more cohesive, such as clay or in clay-silt suspensions, particle damage is negligible so that the gravel retains its initial characteristics during the flow. This study suggests that changes to the morphology of fresh gravel during

landslides are limited as long as there is no severe particle breakage (splitting).

Acknowledgements

The authors acknowledge the financial support provided by the Research Grants Council of HKSAR (17200114, TR22-603-15N) and National Natural Science Foundation of China (42177154, 41402279). Many thanks to Professor Gong-Hui Wang (Disaster Prevention Research Institute, Kyoto University) for commenting this paper.

References

Adams, J., 1978. Data for New Zealand pebble abrasion studies. New Zealand of Science 21, 607-610.

Agung, M.W., Sassa, K., Fukuoka, H., Wang, G., 2004. Evolution of shear-zone structure in undrained ring-shear tests. Landslides 1, 101–112.

Allam, L.M., Ebrahimpour, A., 2014. Comparative analysis of Idaho and Micro-Deval aggregate degradation test methods. Journal of Materials in Civil Engineering 26(1), 198-201.

Anochie-Boateng, J.K., Komba, J.J., Mvelase, G.M., 2013. Three-dimensional laser scanning technique to quantify aggregate and ballast shape properties. Construction and Building Materials 43, 389-398.

Altuhafi, F.N., Coop, M.R., 2011. Changes to particle characteristics associated with the compression of sands. Géotechnique 61(6), 459–471.

Ansari, S.A., Kothyari, U.C., Raju, K.G.R., 2003. Influence of cohesion on scour under submerged circular vertical jets. Journal of Hydraulic Engineering 129(12), 1014-1019.

Arabnia, O., 2015. Particle size reduction in debris flows: laboratory experiments compared to field data from Inyo Greek. MSc thesis, San Francisco University, U.S.

Barret, P.J., 1980. The shape of rock properties, a critical review. Sedimentology 27, 291-303.

Blott, S.J., Pye, K., 2008. Particle shape: a review and new methods of characterization and classification. Sedimentology 55, 31-63.

Caballero, L., Sarocchi, D., Borselli, L., Cárdenas, A.I., 2012. Particle interaction inside debris flows: Evidence through experimental data and quantitative clast shape analysis. J. Volcanol. Geotherm. Res. 231-232, 12–23.

Caballero, L., Sarocchi, D., Soto, E., Borselli, L., 2014. Rheological changes induced by clast fragmentation in debris flows. Journal of Geophysical Research: Earth Surface 119(9), 1800-1817.

Chen, Z., He, S., 2020. Simulation of effects of particle breakage on sliding surface friction for a hypothetical soil continuum moving on an inclined plane. Landslides 17, 2113-2124.

Cho, G.C., Dodds, J., Santamarina, J.C., 2006. Particle shape effects on packing density, stiffness, and strength: natural and crushed sands. Journal of Geotechnical and Geoenvironmental Engineering 132(5), 591-602.

Chou, H.T., Chou, S.H., Hsiau, S.S., 2014. The effects of particle density and interstitial fluid viscosity on the dynamic properties of granular slurries in a rotating drum. Powder technology 252, 42-50.

Cruden, D.M., 1991. A simple definition of a landslide. Bulletin of the International Association of Engineering Geology 43, 27–29.

Cruden, D. M., Varnes, D. J., 1996. Landslide types and processes. In: Turner AK, Schuster RL (eds) Landslides investigation and mitigation. Transportation research board, US National Research Council. Special Report 247, Washington, DC, Chapter 3, 36–75.

Czinder, B., Vásárhelyi, B., Török, Á., 2021. Long-term abrasion of rocks assessed by micro-Deval tests and estimation of the abrasion process of rock types based on strength parameters. Engineering Geology 282, 105996.

Davies, T.R., McSaveney, M.J., 2009. The role of rock fragmentation in the motion of large landslides. Engineering Geology 109 (1-2), 67-79.

Fonseca, J., O'Sullivan, C., Coop, M.R., Lee, P.D., 2012. Non-invasive characterization of particle morphology of natural sands. Soils and Foundations 52(4), 712-722.

Gerolymos, N., & Gazetas, G., 2007. A model for grain-crushing-induced landslides—Application to Nikawa, Kobe 1995. Soil Dynamics and Earthquake Engineering, 27(9), 803-817.

Hungr, O., Leroueil, S., Picarelli, L., 2014. The Varnes classification of landslide types, an update. Landslides 11 (2), 167-194.

Iverson, R. M., 2003. The debris-flow rheology myth. Debris-flow hazards mitigation: mechanics, prediction, and assessment, 1, 303-314.

Iverson, R. M., George, D. L., 2014. A depth-averaged debris-flow model that includes the effects of evolving dilatancy. I. Physical basis. Proceedings of the Royal Society A: Mathematical, Physical and Engineering Sciences 470 (2170), 20130819.

Jain, N., Ottino, J.M., Lueptow, R.M., 2005. Regimes of segregation and mixing in combined size and density granular systems: an experimental study, Granul. Matter 7 (2005), 69–81.

Juarez, G., Chen, P., Lueptow, R. M., 2011. Transition to centrifuging granular flow in rotating tumblers: A modified Froude number. New Journal of Physics 13(5), 053055.

Jing, L., Kowk, C.Y., Leung, Y.F., Zhang, Z., Dai, L., 2018. Runout scaling and deposit morphology of rapid mudflows. Journal of Geophysical Research: Earth Surface 123(8), 2004-2023.

Kaitna, R., Rickenmann, D., 2007. A new experimental facility for laboratory debris flow investigation. Journal of Hydraulic Research 45(6), 797-810.

Lanaro, F., Tolppanen, P., 2002. 3D characterization of coarse aggregates. Engineering Geology 65(1), 17-30.

Lewin, J., Brewer, P.A., 2002. Laboratory simulation of clast abrasion. Earth Surface Process and Landforms 27(2), 145-164.

Li, K.M., Zuo, L., Nardelli, V., Alves, T.M., Lourenco, S.D.N., 2019. Morphometric signature of sediment particles reveals the source and emplacement mechanisms of submarine landslides. Landslides 16, 829–837.

Lin, H., Lourenco, S.D., 2020. Physical degradation of hydrophobized sands. Powder Technology 367, 740-750.

Longo, S., Lamberti, A., 2002. Grain shear flow in a rotating drum. Experiments in Fluids 32, 313–325.

Lumb, P., 1983. Engineering properties of fresh and decomposed igneous rocks from Hong Kong. Engineering Geology 19(2), 81-94.

Masad, E., Kassem, E., Little, D., 2011. Characterization of Asphalt pavement materials in the state of Qatar. Road Materials and Pavement Design 12 (4), 739-765.

Mellmann, J., 2001. The transverse motion of solids in rotating cylinders-forms of motion and transition behavior. Powder Technology 118, 251-270.

Mitchell, J.K., Soga, K., 2005. Fundamentals of Soil Behavior. NJ: John Wiley & Sons.

Nayak, P. R., 1971. Random process model of rough surfaces. Journal of Lubrication Technology 93(3), 398-407.

Ng, C.W.W., Liu, H., Choi, C.E., Kwan, J.S.H., Pun, W.K., 2021. Impact dynamics of boulder-enriched debris flow on a rigid barrier. J Geotech Geoenviron (ASCE), 147(3), 04021004

Ngan-Tillard, D., Haan, J., Laughton, D., Mulder, A., van der Kolff, A.N., 2009. Index test for the degradation potential of carbonate sands during hydraulic transportation. Engineering Geology 108(1-2), 54-64.

Otsubo, M., O'Sullivan, C., Sim, W.W., Ibraim, E., 2015. Quantitative assessment of the influence of

surface roughness on soil stiffness. Géotechnique 65(8), 694-700.

Perinotto, H., Schneider, J. L., Bachèlery, P., Le Bourdonnec, F. X., Famin, V., Michon, L. 2015. The extreme mobility of debris avalanches: A new model of transport mechanism. Journal of Geophysical Research: Solid Earth 120(12), 8110-8119.

Rousé, P.C., Fannin, R.J., Shuttle, D. A., 2008. Influence of roundness on the void ratio and strength of uniform sand. Géotechnique 58(3), 227-231.

Santos, D. A., Duarte, C. R., Barrozo, M. A. S., 2016. Segregation phenomenon in a rotary drum: experimental study and CFD simulation. Powder Technology 294, 1-10.

Sassa, K., 1998. *Mechanisms of landslide triggered debris flows*. In: Sassa K. (eds) Environmental Forest Science. Forestry Sciences, 54. Springer, Dordrecht.

Schneider, D., Kaitna, R., Dietrich, W. E., Hsu, L., Huggel, C., & McArdell, B. W., 2011. Frictional behavior of granular gravel–ice mixtures in vertically rotating drum experiments and implications for rock–ice avalanches. Cold Regions Science and Technology 69(1), 70-90.

Sewell RJ, 1999. Geochemical atlas of Hong Kong, Geotechnical Engineering Office, Civil Engineering Dept., Hong Kong, 110 pp.

Woodside, A.R., Woodward, W.D.H., 1998. Assessing the wear characteristics of aggregate exposed at the road surface. Geological Society, London, Engineering Geology Special Publications 13(1), 149-157.

Yang, H., Baudet, B.A., Yao, T., 2016. Characterization of the surface roughness of sand particles using an advanced fractal approach. Proceedings of the Royal Society of London A 472(2194).

Yang, H., Lourenco, S.D.N., Baudet, B.A., Choi, C.E., Ng., C.W.W., 2019. 3D analysis of gravel surface texture. Powder Technology 346, 414-424.

Yang, K., Xu, Z. M., Tian, L., Wang, K., Ren, Z., Tang, Y. J., Gao, H. Y., 2020. Significance of coarse clasts in viscous debris flows. Engineering Geology 272, 105665.

Yao, T., Baudet, B.A., Lourenço, S.D.N., 2019. Quantification of the surface roughness of quartz sand using optical interferometry. Meccanica 54, 741–748.

Yao, T., Baudet, B.A., Lourenço, S.D.N., 2021. Evolution of surface roughness of single sand grains with normal loading. Géotechnique, https://doi.org/10.1680/jgeot.20.P.310.

Yu, F., Zhang, C., Xie, Q., Su, L., Zhao, T., & Jan, M. Q., 2020. Particle breakage of sand subjected to friction and collision in drum tests. Journal of Rock Mechanics and Geotechnical Engineering.

Zhao, B., Wang, J., 2016. 3D quantitative shape analysis on form, roundness, and compactness with

μCT. Powder Technology 291, 262-275.

Zheng, S., Lourenco, S.D.N., Cleall, P.J., Ng, A., 2019. Erodibility of synthetic water repellent granular materials: Adapting the ground to weather extremes. Science of the Total Environment 689, 398-412.

Zingg, T., 1935. Beitrag zur schotteranalyse, Schweiz. Mineral. Petrogr. Mitt 15, 52-56.

Zuo, L., Lourenco, S.D.N., Baudet, B.A., 2019. Experimental insight into the particle morphology changes associated with landslide movement. Lanslides 16, 787–798.

Table 1. Testing programme

Test	Mass/g						Solid concentration (%)	Revolutions
	Granite gravel	Water	Clay	Silt	Steel balls	Total mass		
RUN 1	414.1	0	0	0	1035.3	1449.4	/	20000, 60000
RUN 2	386.0	0	0	0	965.0	1351	/	20000, 60000
RUN 3	361.1	540	0	0	902.8	1803.9	46.5	20000, 60000
RUN 4	395.3	600	320	0	988.3	2303.6	66.3	20000, 60000
RUN 5	377.1	570	0	271	942.8	2160.9	63.8	20000, 60000

Table 2. Mean values and standard deviation (SD) of mass, particle size and morphological parameters of gravel. Note: EI is the elongation index; FI represents the flatness index; R is the roundness calculated by Eq. 1; DPSD is the fractal dimension obtained by Eq. 3.

Test	Revolutions	Mass /g	Diameter /mm	EI	FI	R	D_{PSD}
RUN 1	0	12.9±2.9	23.98±5.78	0.81±0.10	0.76±0.14	0.62±0.03	2.561±0.033
	20000	12.5±2.8	23.42±5.62	0.80±0.11	0.76±0.14	0.64±0.03	2.561±0.028
	60000	12.2±2.8	23.01±5.54	0.81±0.11	0.77±0.13	0.65±0.04	2.560±0.025
RUN 2	0	12.1±2.5	23.93±7.55	0.72±0.15	0.75±0.12	0.61±0.03	2.574±0.019
	20000	11.6±2.5	23.30±7.29	0.72±0.15	0.77±0.13	0.64±0.03	2.573±0.033
	60000	11.1±2.4	23.16±7.42	0.70±0.14	0.76±0.12	0.66±0.03	2.574±0.026
RUN 3	0	11.3±1.9	24.00±6.61	0.73±0.12	0.77±0.15	0.61±0.03	2.572±0.022
	20000	10.9±2.6	22.56±6.01	0.73±0.12	0.77±0.12	0.65±0.03	2.571±0.025
	60000	10.0±2.6	21.84±5.95	0.73±0.12	0.76±0.13	0.67±0.03	2.568±0.018
RUN 4	0	12.4±2.0	24.18±6.42	0.76±0.12	0.75±0.13	0.62±0.03	2.568±0.025
	20000	12.2±1.9	23.69±6.30	0.76±0.13	0.76±0.13	0.62±0.03	2.567±0.022
	60000	12.1±1.9	23.59±6.36	0.76±0.13	0.75±0.13	0.63±0.04	2.567±0.027
RUN 5	0	11.8±1.8	23.71±7.06	0.71±0.13	0.76±0.12	0.62±0.03	2.567±0.022
	20000	11.5±1.8	22.92±6.87	0.70±0.12	0.77±0.12	0.63±0.03	2.577±0.025
	60000	11.2±1.7	22.68±6.72	0.71±0.12	0.78±0.13	0.65±0.03	2.570±0.023

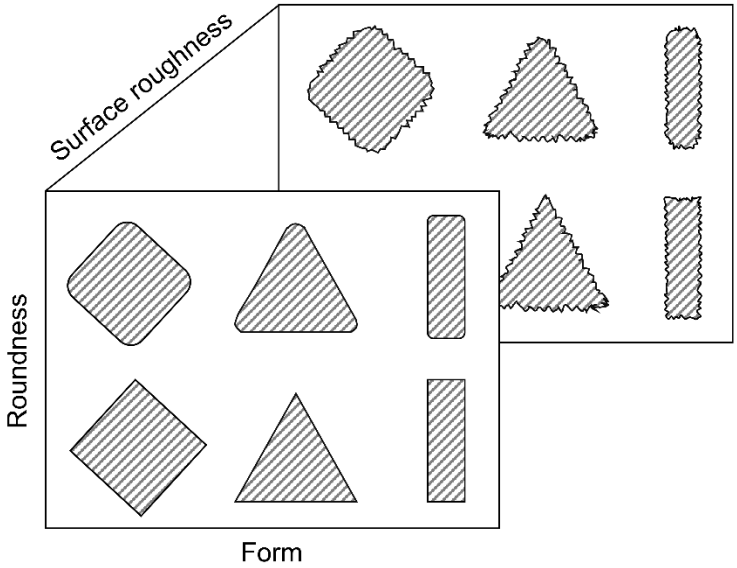

Figure 1. Schematic illustration of the three scales of particle morphology (*after* Barret, 1980)

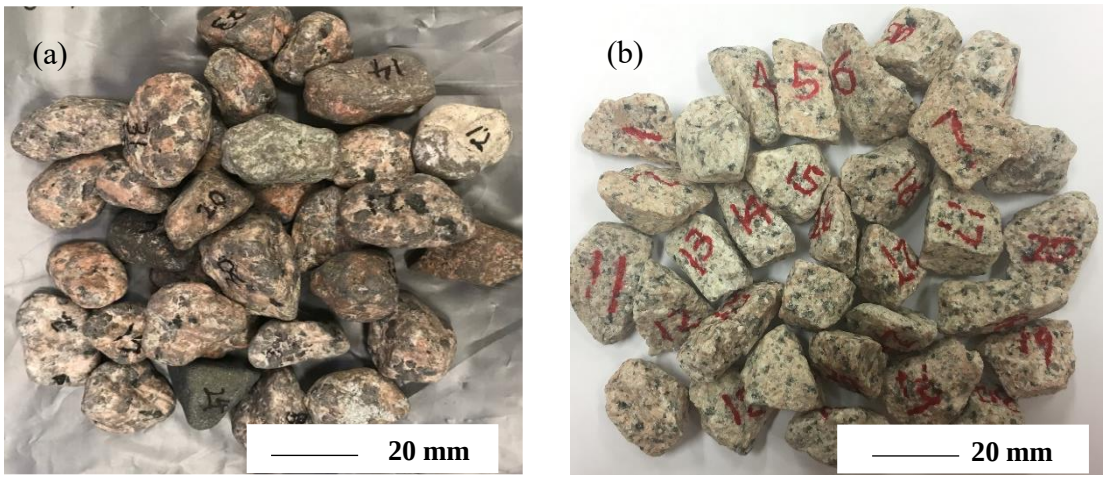

Figure 2. Numbered gravel grains used in the tests: a) RUN 1; b) RUN 2 to RUN 5

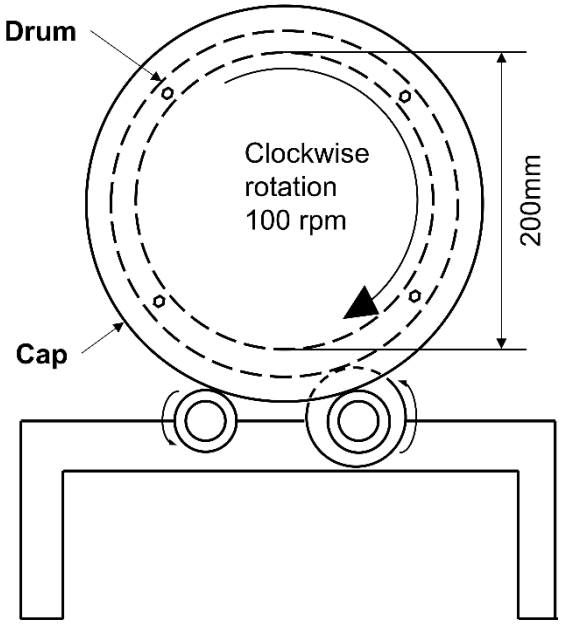

Figure 3. Schematic illustration of the Micro-Deval abrasion apparatus

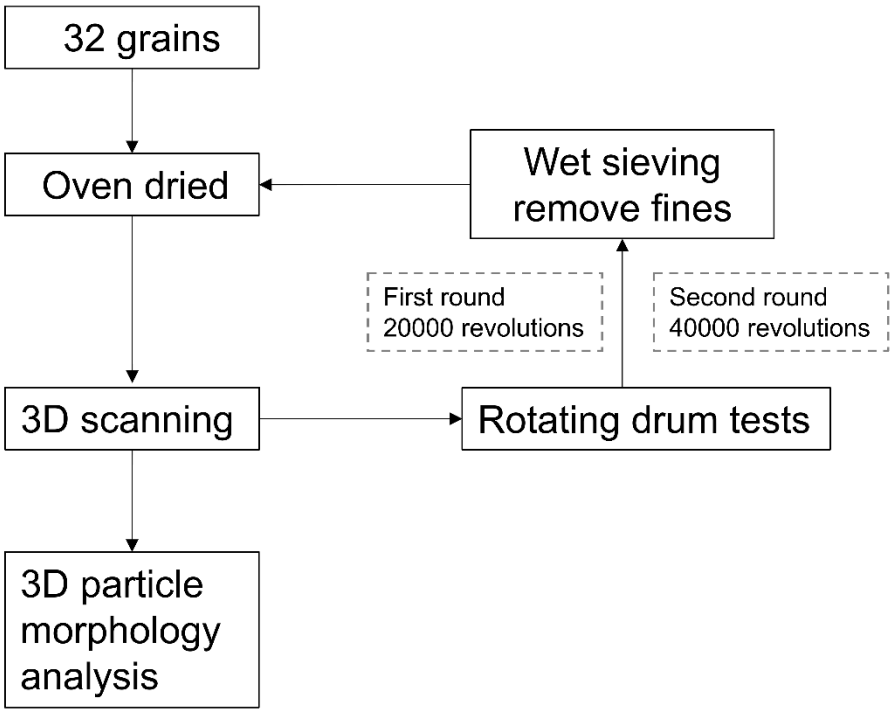

Figure 4. Schematic illustration of the experimental workflow

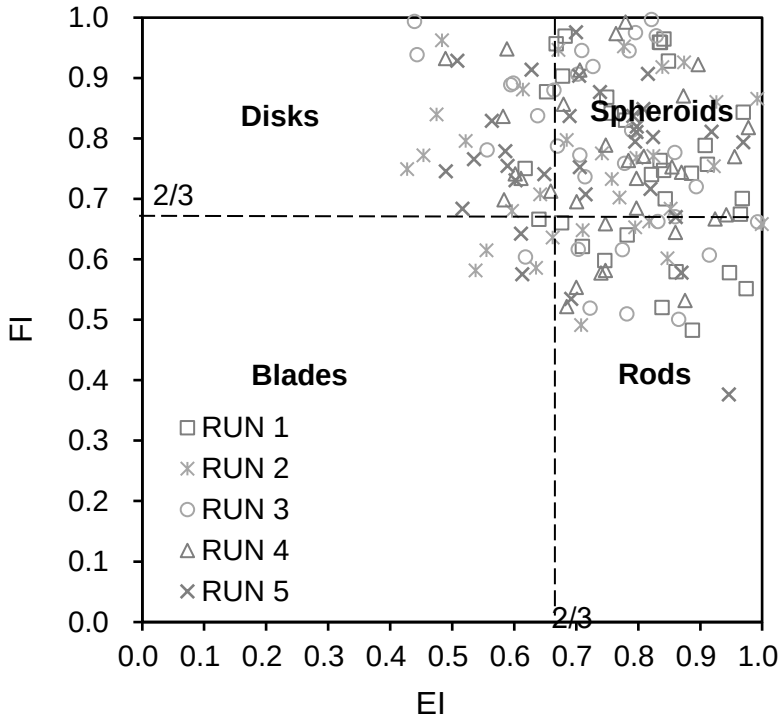

Figure 5. Aspect ratios of the gravel before test (EI: elongation index; FI: flatness index)

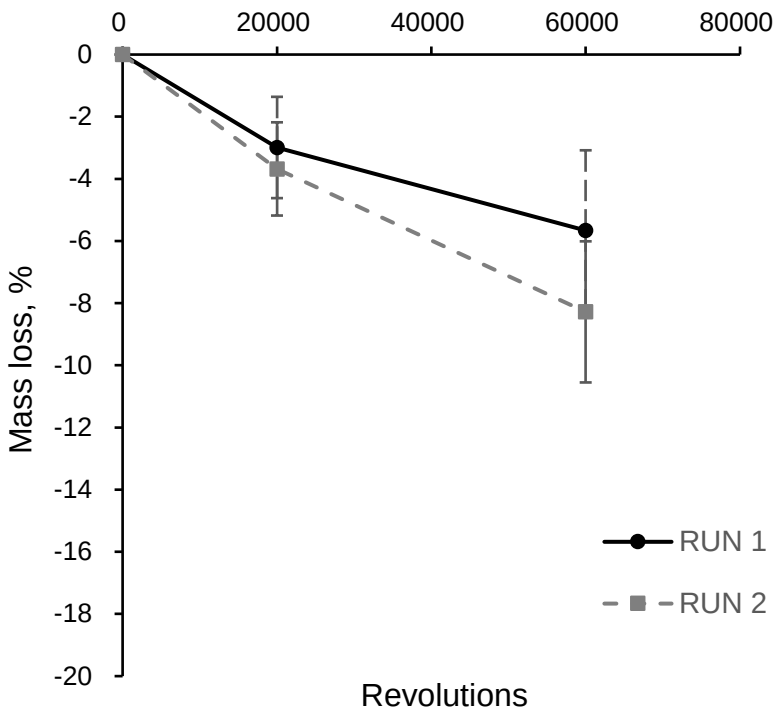

Figure 6. Evolution of mass loss of gravel with revolutions in a dry condition for RUN 1 and RUN 2

(a)

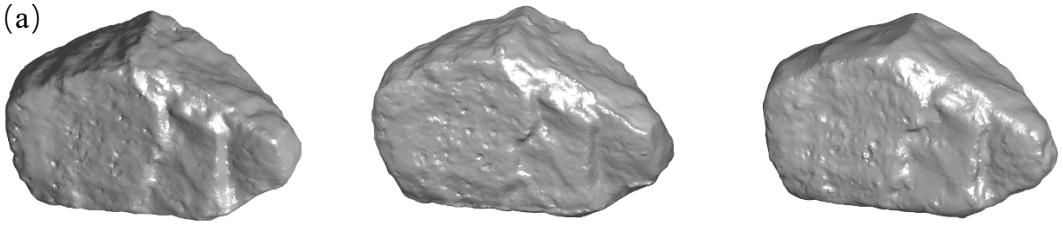

Before test		Revolutions (20000)		Revolutions (60000)	
Mass, g	13.65	Mass, g	13.52	Mass, g	13.46
Diameter, mm	24.40	Diameter, mm	24.31	Diameter, mm	24.13
EI	0.684	EI	0.674	EI	0.688
FI	0.522	FI	0.527	FI	0.547
Roundness	0.67	Roundness	0.69	Roundness	0.70
Fractal dimension	2.591	Fractal dimension	2.587	Fractal dimension	2.579

(b)

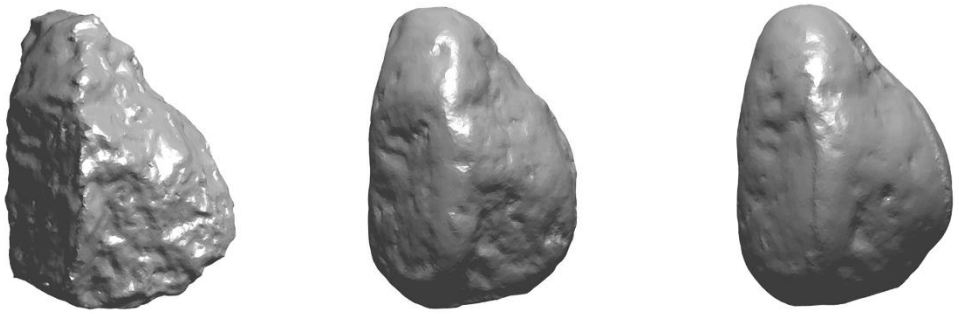

Before test		Revolutions (20000)		Revolutions (60000)	
Mass, g	11.52	Mass, g	9.53	Mass, g	8.24
Diameter, mm	23.87	Diameter, mm	20.92	Diameter, mm	19.73
EI	0.73	EI	0.71	EI	0.71
FI	0.92	FI	0.94	FI	0.90
Roundness	0.62	Roundness	0.70	Roundness	0.71
Fractal dimension	2.563	Fractal dimension	2.537	Fractal dimension	2.519

Figure 7. Examples of the change of particle morphology of a single gravel grain at different revolutions: a) a particle from RUN 1 (mass loss 1.4%); b) a particle from RUN 3 with maximum mass loss (28%) among 160 particles

(a)

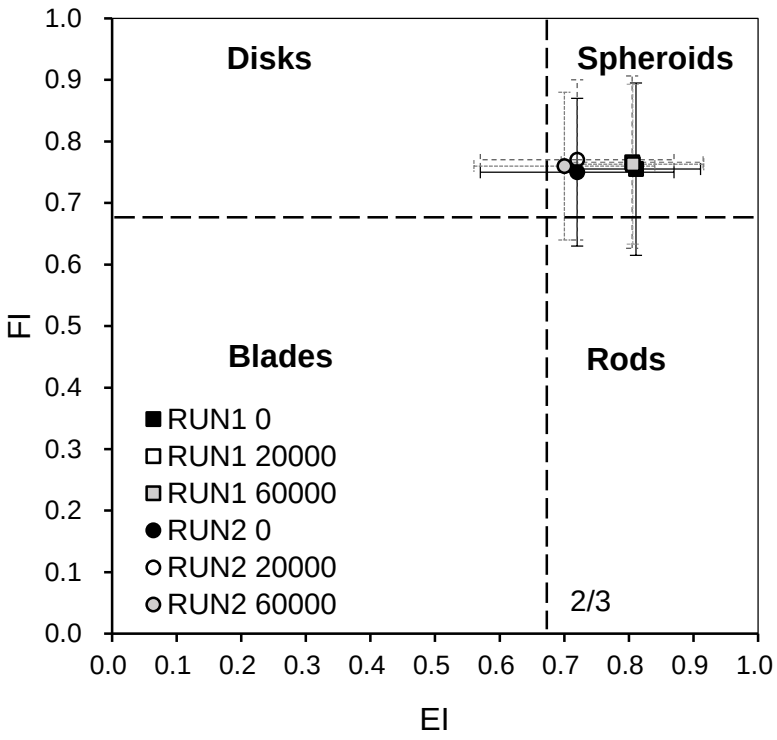
Disks
Spheroids
Blades
Rods
2/3
RUN1 0
RUN1 20000
RUN1 60000
RUN2 0
RUN2 20000
RUN2 60000
FI
EI
0.0
0.1
0.2
0.3
0.4
0.5
0.6
0.7
0.8
0.9
1.0

(b)

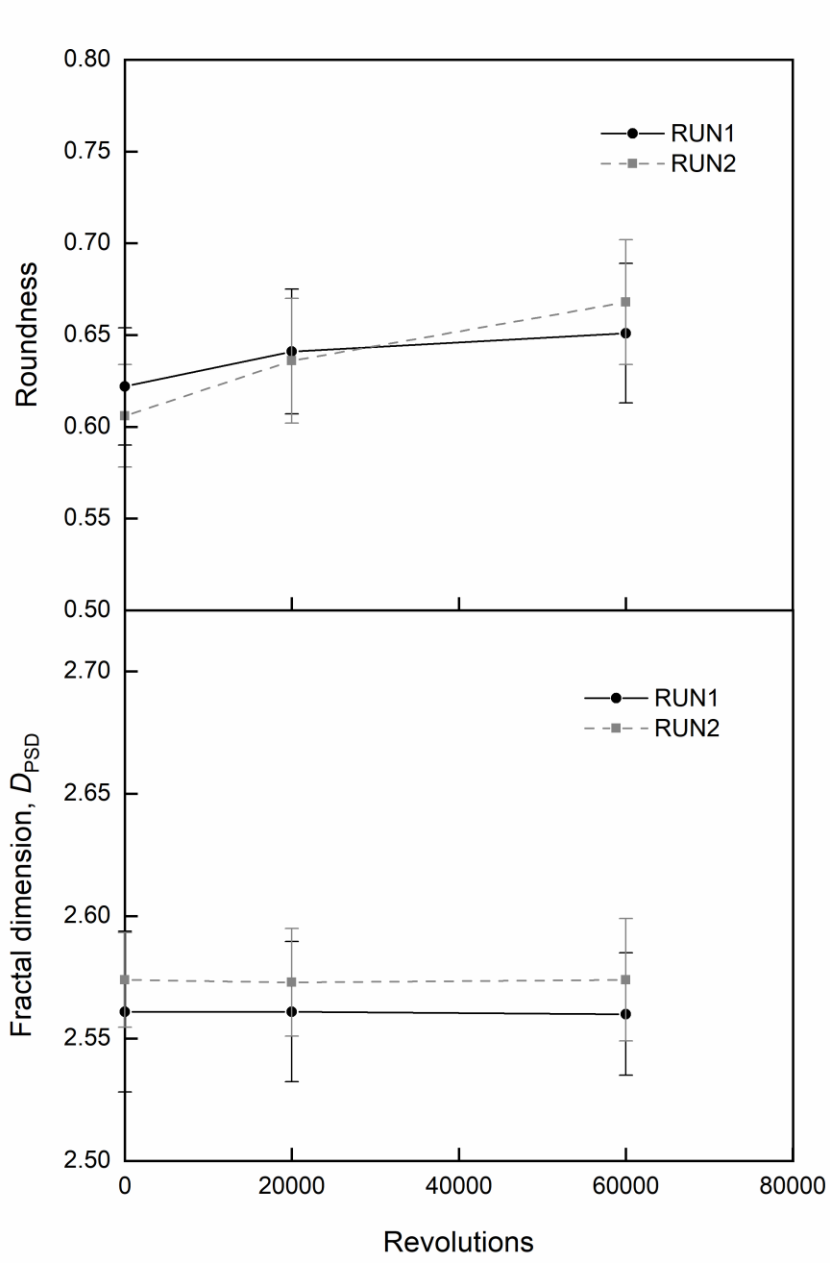

Figure 8. Evolution of particle morphology with revolutions in a dry condition for RUN 1 and RUN 2: a) aspect ratios (EI and FI); b) roundness and fractal dimension

(a)

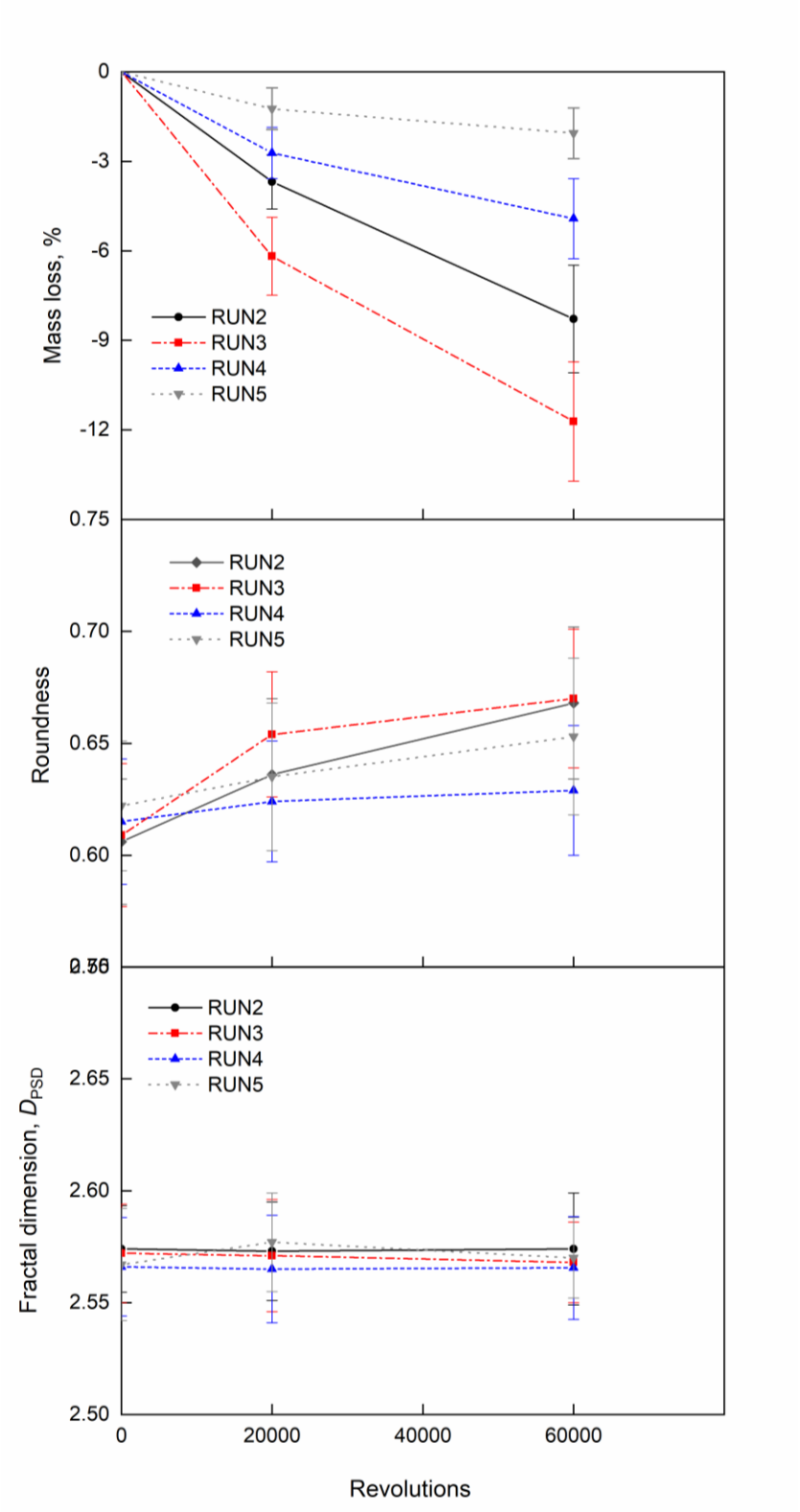
Mass loss, %
0
-3
-6
-9
-12
RUN2
RUN3
RUN4
RUN5
Roundness
0.75
0.70
0.65
0.60
RUN2
RUN3
RUN4
RUN5
Fractal dimension, D_{PSD}
2.65
2.60
2.55
2.50
RUN2
RUN3
RUN4
RUN5
0
20000
40000
60000
Revolutions

(b)

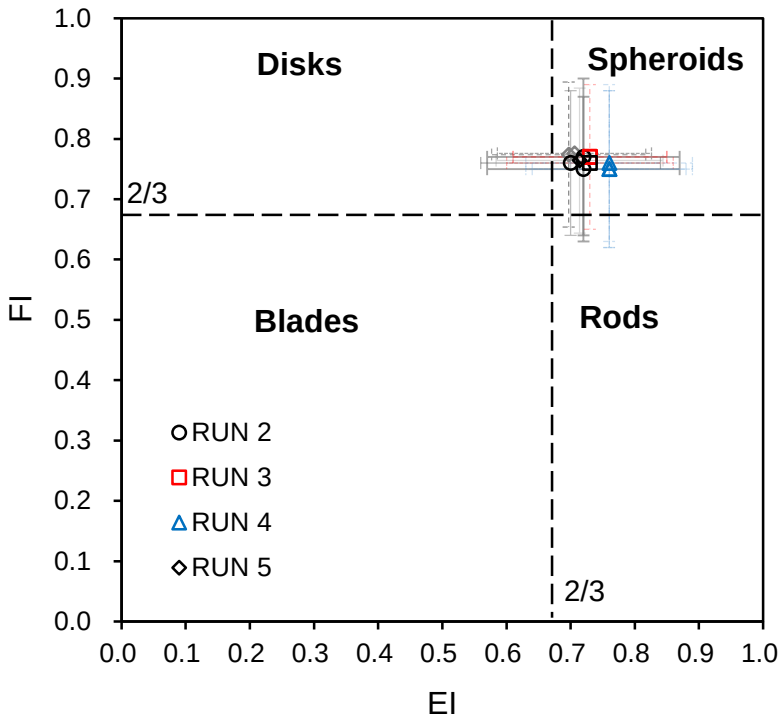

Figure 9. Evolution of mass loss and particle morphology with revolutions for angular grains in a dry condition (RUN 2), saturated with water (RUN 3), with clay (RUN 4) and silt (RUN 5): a) Mass loss, roundness, and fractal dimension; b) aspect ratios (EI and FI)

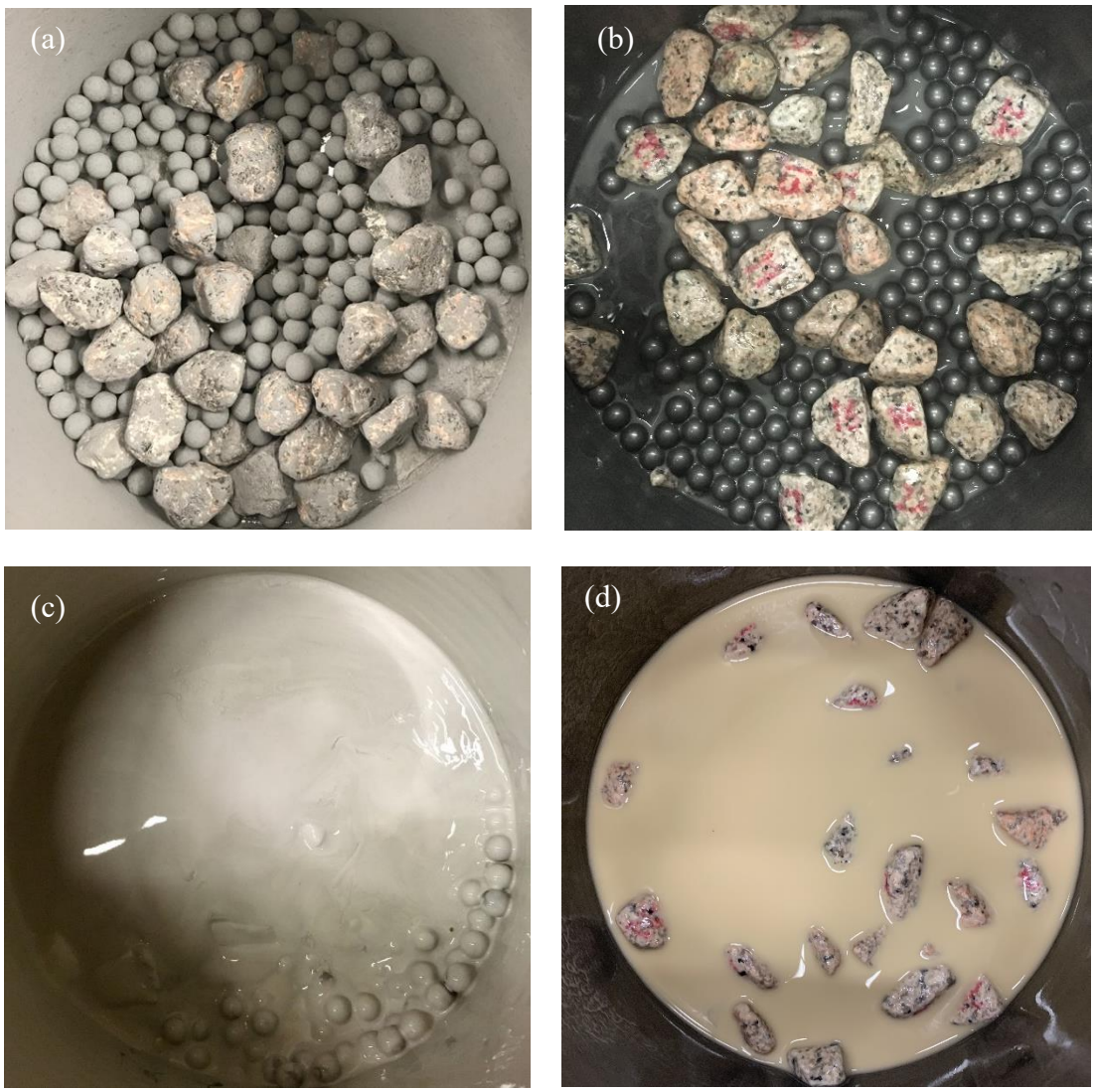

Figure 10. Angular grains after 20000 revolutions: a) tested in dry condition (RUN 2); (b) saturated with water (RUN 3); (c) saturated with clay-slurry (RUN 4); (d) saturated with silt-slurry (RUN 5) (each gravel grain has a diameter 20-30 mm)